

Accepted Manuscript

H₅PW₁₀V₂O₄₀@VO_x/SBA-15-NH₂ catalyst for the solventless synthesis of 3-substituted indoles

Narges Mahdizadeh ghohe, Reza Tayebee, Mostafa M. Amini, Amin Osatiashtiani, Mark A. Isaacs, Adam F. Lee

PII: S0040-4020(17)30861-X

DOI: [10.1016/j.tet.2017.08.030](https://doi.org/10.1016/j.tet.2017.08.030)

Reference: TET 28924

To appear in: *Tetrahedron*

Received Date: 26 May 2017

Revised Date: 31 July 2017

Accepted Date: 14 August 2017

Please cite this article as: Mahdizadeh ghohe N, Tayebee R, Amini MM, Osatiashtiani A, Isaacs MA, Lee AF, H₅PW₁₀V₂O₄₀@VO_x/SBA-15-NH₂ catalyst for the solventless synthesis of 3-substituted indoles, *Tetrahedron* (2017), doi: 10.1016/j.tet.2017.08.030.

This is a PDF file of an unedited manuscript that has been accepted for publication. As a service to our customers we are providing this early version of the manuscript. The manuscript will undergo copyediting, typesetting, and review of the resulting proof before it is published in its final form. Please note that during the production process errors may be discovered which could affect the content, and all legal disclaimers that apply to the journal pertain.

H₅PW₁₀V₂O₄₀@VO_x/SBA-15-NH₂ catalyst for the solventless synthesis of 3-substituted indoles

Narges Mahdizadeh ghohe^a, Reza Tayebee^{*a}, Mostafa M. Amini^b, Amin Osatiashtiani^c, Mark A. Isaacs^c, Adam F. Lee^c

^a*Department of Chemistry, School of Sciences, Hakim Sabzevari University, Sabzevar 96179-76487, Iran*

^b*Department of Chemistry, Shahid Beheshti University, G.C., Tehran 1983963113, Iran*

^c*European Bioenergy Research Institute, Aston University, Birmingham B4 7ET, UK*

*Corresponding author: Email: Rtayebee@hsu.ac.ir; Tel: +98-51-44410310

Abstract

Functionalization of mesoporous SBA-15 frameworks by transition metal oxides offers a flexible route to fabricate new heterogeneous catalysts. Here, an inorganic-organic hybrid nanoporous catalyst H₅PW₁₀V₂O₄₀@VO_x/SBA-15-NH₂, was prepared and utilized as an efficient, eco-friendly, and recyclable catalyst for the one-pot, multi-component synthesis of 3-substituted indoles by indole substitution with aldehydes and malononitrile under solvent-free conditions. Catalysts were prepared by the non-covalent attachment of H₅PW₁₀V₂O₄₀ to a 3 wt% VO_x/SBA-15 nanoporous support through a 3-(triethoxysilyl)propylamine linker. VO_x/SBA-15 was prepared by a one-pot hydrothermal synthesis from TEOS and vanadium(V) oxytri-tert-butoxide [VO(O-^tBu)₃]. The resulting H₅PW₁₀V₂O₄₀@VO_x/SBA-15-NH₂ material was characterized by bulk and surface analysis including N₂ porosimetry, FE-SEM, XRD, XPS, FT-IR, TGA-DTA, UV-Vis and ICP-OES, evidencing retention of the heteropolyacid Keggin structure. H₅PW₁₀V₂O₄₀@VO_x/SBA-15-NH₂ exhibits high activity and excellent yields (70-95 %) of 3-substituted indoles under mild conditions, with negligible deactivation.

Keywords: Vanadia; SBA-15; heteropolyacid; 3-Substituted indoles; Solventless

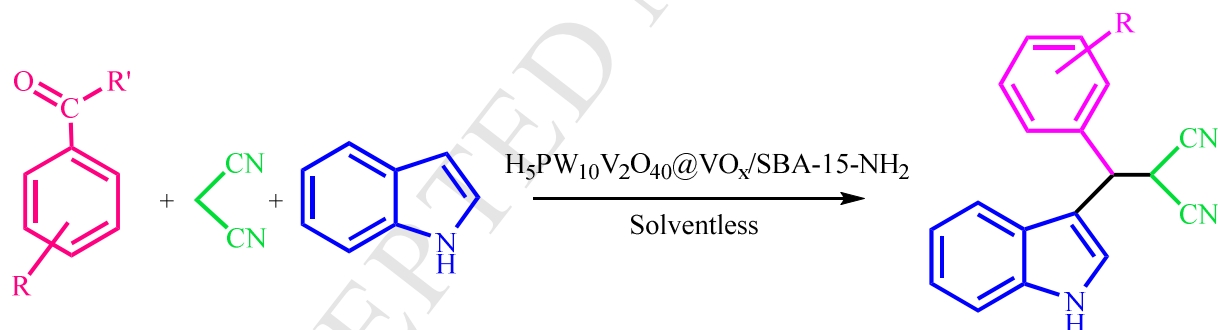
1. Introduction

Mesoporous molecular sieves M41S with uniform pore sizes exceeding 20 Å and surface areas reaching 1000 m²g⁻¹ have proven to be valuable architectures for applications in heterogeneous catalysis, notably the genesis of solid acids and associated organic transformations.¹⁻⁴ Among mesoporous silicas, SBA-15 has attracted considerable attention due to its large and tunable pore dimensions, thick walls and hence good hydrothermal stability, and flexible adaptation into hierarchical frameworks.⁵ Despite the lack of lattice defects, limited redox or basicity/acidity of pure SBA-15, such physicochemical properties can be readily modified through the introduction of inorganic and/or organic species either into the silica framework or over its surface to generate new catalytically active sites.⁶⁻¹²

Various transition metals can be introduced into the siliceous frameworks,^{1,13} including vanadium to yield vanadia-functionalized mesoporous MCM-41¹³ and SBA-15^{14,15} frameworks for oxidation and acid catalysis,^{14,16-18} with high-valent vanadia species increasing SBA-15 acidity.^{19,20} A high concentration of vanadium, in a range of oxidation states, can be incorporated into SBA-15 without destroying the mesoporous framework.¹ Indeed, vanadium functionalized mesoporous silicas (e.g. V-SBA-15, V-MCM-41, V-MCM-48, V-MCF) often exhibit uniform pore sizes and high surface areas, and consequently a high density of accessible (and well-defined) active VO_x centers.^{9,21-27} Direct incorporation of metal ions within the silica framework of SBA-15 is challenging and requires strong acidic conditions,^{9,28,29} and the majority of such approaches employ post-synthetic grafting of SBA-15 and/or complex experimental conditions; new approaches to introduce and control the oxidation state of vanadium within mesoporous SBA-15 are therefore desirable. In this context, vanadium(V) oxytri-tert-butoxide (OV(O^tBu)₃) is known to generate V₂O₅ clusters under acidic conditions and hence offers a means to attach isolated, tetrahedral vanadium(V) species to silica surfaces via Si-O-V bonds.⁹ The loading, cluster size and oxidation state of various transition metals is known to strongly influence the activity of doped silica catalysts.^{30,31} Heteropolyacids (HPAs) are polyoxometalate inorganic cages which possess tunable (and even superacidic) Brønsted acidity.³² HPAs can be readily incorporated into mesoporous silicas to promote acid catalyzed transformations such as terpene isomerization, wherein SBA-15 was recently shown to stabilize highly dispersed H₃PW₁₂O₄₀ clusters improving acid site densities and accessibility,³³ and the Biginelli condensation of substituted aldehydes with ethyl acetoacetate and urea to form 3,4-

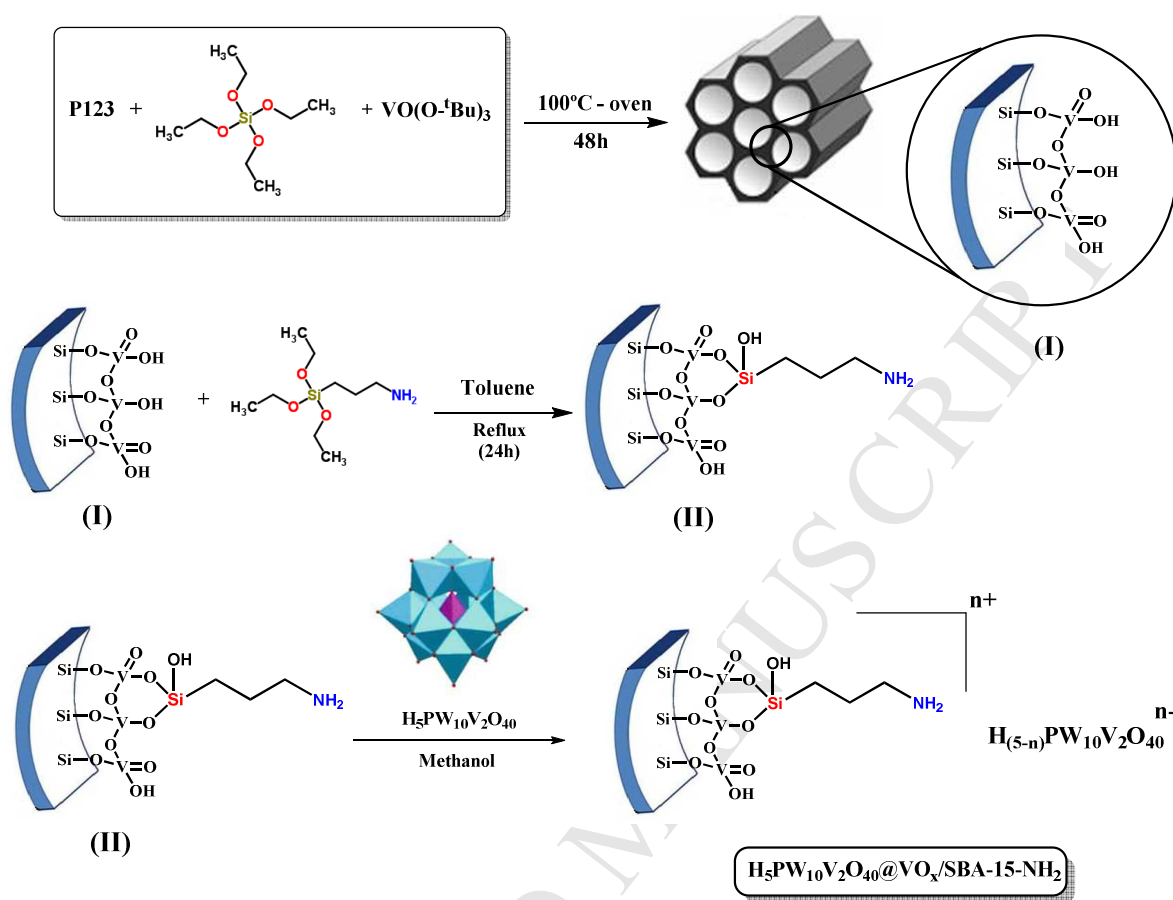
dihydropyrimidin-2-(1H)-ones over piperazine tethered $H_5PW_{10}V_2O_{40}$.³⁴ 3-Substituted indoles are important chemical intermediates and pharmaceutical precursors³⁵ and pharmacologically active analogues of synthetic Ergine, Gramine, and Sumatriptan production, and as aromatase and integrase inhibitors for breast cancer and HIV-1 therapies, respectively.³⁶ Existing protocols for the preparation of substituted indoles such as 2-((1H-indol-3-yl)(phenyl)methyl)malononitrile suffer from disadvantages including long reaction times, high temperatures and the requirement for stoichiometric catalyst quantities, or deliver unsatisfactory yields or utilize homogeneous catalysts with associated product separation issues.³⁷⁻⁴⁰ New active, low cost catalysts employing earth abundant elements are thus sought for operation under mild reaction conditions.

Herein, we describe a simple and efficient direct route to introduce vanadium into SBA-15 by adjusting the pH during a sol-gel synthesis step,^{9,41,28,42,43} and modifying the resulting $VO_x/SBA-15$ surface with a 3-(triethoxysilyl)propylamine linker to subsequently non-covalently bind $H_5PW_{10}V_2O_{40}$. The resulting hybrid nanoporous material exhibits Lewis/Brønsted solid acid character and the associated catalytic activity for the one-pot, multi-component synthesis of 3-substituted indoles (**Scheme 1**). Immobilization of the HPA component through electrostatic interactions suppresses catalyst leaching and hence improves recyclability.



R= halogen, nitro, methoxy; R'= H

Scheme 1. One-pot synthesis of 3-substituted indoles from indole, malononitrile and aldehydes.



Scheme 2. Preparation of $\text{H}_5\text{PW}_{10}\text{V}_2\text{O}_{40}@/\text{VO}_x/\text{SBA-15-NH}_2$.

2. Results and discussion

2.1. Structure of functionalized SBA-15

Elemental analysis by ICP-OES demonstrated the actual V loading of the $\text{VO}_x/\text{SBA-15}$ and $\text{VO}_x/\text{SBA-15-NH}_2$ materials as 3.7 and 3 wt%, respectively. Textural properties of the functionalized mesoporous SBA-15 silicas were characterized by porosimetry and the resulting adsorption-desorption isotherms shown in **Figure 1** and corresponding surface areas and pore volumes summarized in **Table 1**. All materials exhibited type IV isotherms characteristic of a conventional SBA-15³³ with type H3 hysteresis loops (indicative of slit-shaped pores),⁴⁴ with dimensions for the as-prepared $\text{VO}_x/\text{SBA-15}$ similar to those reported for SBA-15, indicating that V incorporation into the sol-gel step had minimal impact on the mesopore structure. The small micropore contribution is often observed in the cooperative self-assembly route employed

in this work, in contrast to true liquid crystal templating routes which offer reduced microporosity.⁴⁵ Amine-grafting, and subsequent HPA incorporation, significantly lowered the surface area and total pore volume relative to VO_x/SBA-15, and eliminated microporosity, yet had negligible impact on the mean mesopore diameter. These changes indicate that both post-functionalization steps induced substantial pore blockage.

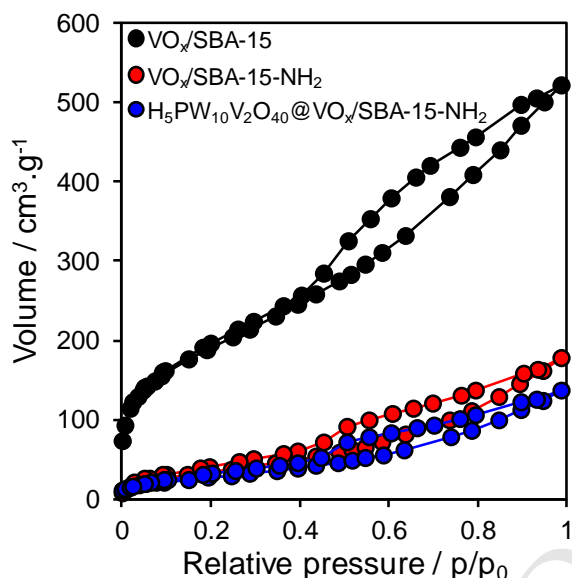


Figure 1. N₂ adsorption-desorption isotherms for functionalized SBA-15.

Table 1. Textural properties of functionalized SBA-15

Sample	BET surface area / m ² .g ⁻¹	BJH pore diameter / Nm	Total pore volume / cm ³ .g ⁻¹	Micropore volume / cm ³ .g ⁻¹
VO _x /SBA-15	695	3.9	0.81	0.015
VO _x /SBA-15-NH ₂	128	3.9	0.28	-
H ₅ PW ₁₀ V ₂ O ₄₀ @VO _x /SBA-15- NH ₂	99	3.8	0.21	-

Crystallinity was subsequently probed by low (**Figure S1**) and wide angle (**Figure 2**) XRD. All three samples exhibited a broad feature between $2\theta = 18^\circ$ and 30° characteristic of the amorphous silica framework. In addition, the parent VO_x/SBA-15 exhibited sharp, but weak, reflections indicative of V₂O₅ (JCPDS card: 41-1426) with d values of 5.75, 4.39, 4.10, 3.41, 2.88, 2.77, 2.61, 2.19, 1.99, 1.92 and 1.78 Å, indicating the presence of a crystalline VO_x phase on the SBA-15 with 60 nm crystallite size according to Scherrer analysis of the peak width,

which must co-exist as a discrete phase, and not within the SBA-15 pore network. However, the low intensity of these V_2O_5 reflections relative to the background indicates that only a small proportion of the 3.7 wt% vanadium incorporated is present in these large crystallites, with the remainder presumably present in smaller particles or clusters (< 2 nm and hence below the instrumental sensitivity limit) dispersed throughout the SBA-15 pore network as depicted in Scheme 2. These reflections were lost following amine functionalization and anchoring of HPA, indicating disruption of the V_2O_5 crystallites, while the absence of $H_5PW_{10}V_2O_{40}$ reflections suggests that the HPA was highly dispersed throughout the 3% $VO_x/SBA-15-NH_2$ material, as observed for low loadings (< 9 wt% W) of $H_3PW_{12}O_{40}$ over unmodified SBA-15³³ and $H_{15}P_5W_{30}O_{110}$ (~ 5 wt%) on the inner surface of modified MCM-41.⁴⁶ The low angle XRD pattern of $HPA@VO_x/SBA-15-NH_2$ shows an intense peak at $2\theta = 0.6^\circ$ evidencing retention of the mesoporous silica framework following functionalization by the amine linker and $H_5PW_{10}V_2O_{40}$. However, higher order reflections expected for the $p6mm$ hexagonal close-packed SBA-15 network^{11,33} were absent, suggesting poor long-range ordering of mesopores, and indeed ordered mesopore arrays could not be imaged by HR-TEM. The absence of higher order reflections and poor long-range ordering probably reflects the in situ synthesis of $VO_x/SBA-15$ in this work; ordered mesopore arrays are only reported for vanadium oxide on SBA-15 prepared by post-synthetic hydrothermal functionalization of the silica support.⁴⁷ XPS revealed V $2p_{3/2}$ binding energies around 515.4 eV for all three materials, consistent with high valent (IV or V) vanadium⁴⁸ and the V_2O_5 phase observed by XRD.

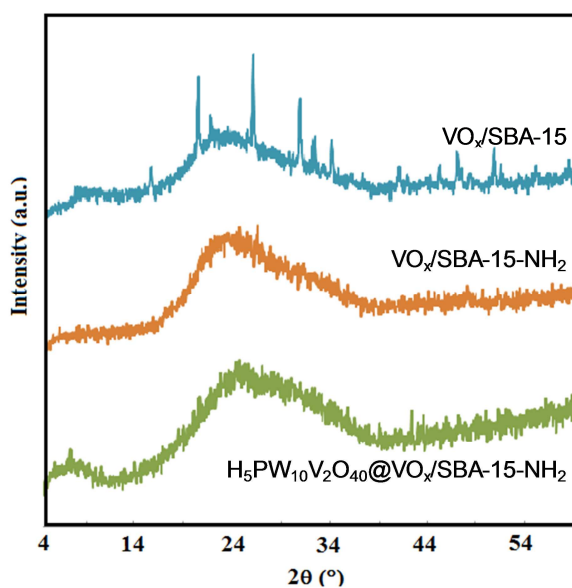


Figure 2. Wide angle XRD patterns of functionalized SBA-15.

Thermogravimetric (TGA-DTA) profiles of the $\text{H}_5\text{PW}_{10}\text{V}_2\text{O}_{40}@VO_x/\text{SBA-15-NH}_2$ performed under air in **Figure 3** reveal a weak endotherm and concomitant small weight loss associated with the desorption of physisorbed water between 50-150 °C. A second, larger weight loss and coincident broad exotherm around 285 °C is most reasonably associated with combustion of the tethered amine, and equates to an amine loading of 2.4 mmol.g^{-1} . A second weak exothermic peak (relative to the sloping baseline) was observed spanning 425-525 °C, coincident with a small mass loss observed in the TGA profile of the parent $\text{H}_5\text{PW}_{10}\text{V}_2\text{O}_{40}$ (**Figure S2**), and hence is attributed to thermal decomposition of the heteropolyacid. The absence of a second mass loss in **Figure 3** associated with the heteropolyacid decomposition in the functionalized silica is not surprising given that this process only accounts for a 2 % mass loss in the parent $\text{H}_5\text{PW}_{10}\text{V}_2\text{O}_{40}$ (which itself only comprises 35 wt% of the composite, see below).

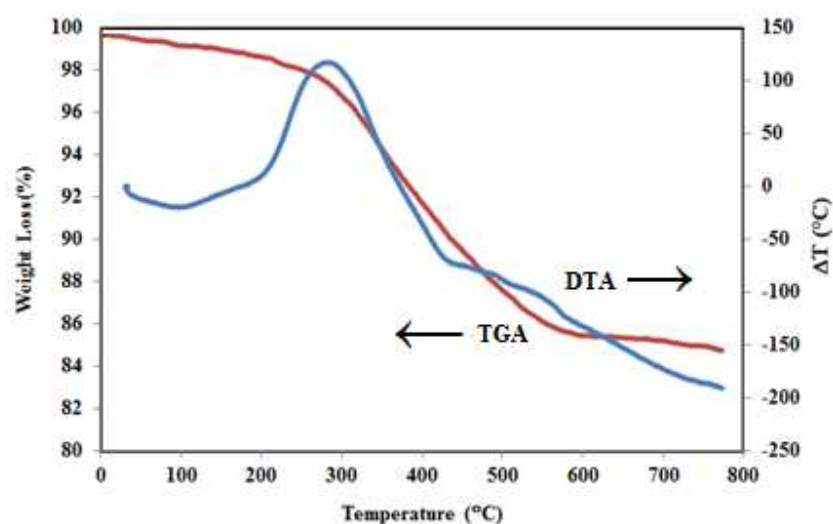


Figure 3. TGA-DTA profiles for $\text{H}_5\text{PW}_{10}\text{V}_2\text{O}_{40}@VO_x/\text{SBA-15-NH}_2$

Electronic properties of the $\text{H}_5\text{PW}_{10}\text{V}_2\text{O}_{40}@VO_x/\text{SBA-15-NH}_2$ sample were explored by UV-Vis spectroscopy during the HPA immobilization step (**Figure 4**): $\text{VO}_x/\text{SBA-15-NH}_2$ (1.0 g)

was suspended in a 60 mL $\text{H}_5\text{PW}_{10}\text{V}_2\text{O}_{40}$ methanolic solution at an initial HPA concentration of 18000 ppm under reflux. UV-Vis spectra of the pure HPA exhibit two ligand \rightarrow metal charge-transfer bands originating from different oxygen species. The strong band around 210 nm is assigned to $\text{O}_d\rightarrow\text{W}$ charge-transfer from the terminal oxygens, while that at 265 nm is assigned to $\text{O}\rightarrow\text{V}$ charge-transfer from the bridging oxygen atoms.⁴⁹ Periodic analysis of aliquots withdrawn from the above solution revealed a systematic decrease in the 265 nm band characteristic of the parent $\text{H}_5\text{PW}_{10}\text{V}_2\text{O}_{40}$, with quantification against calibration curves evidencing a final HPA loading of 0.14 mmol g^{-1} (~37 wt%) in excellent agreement with ICP-OES (35.1 wt%).

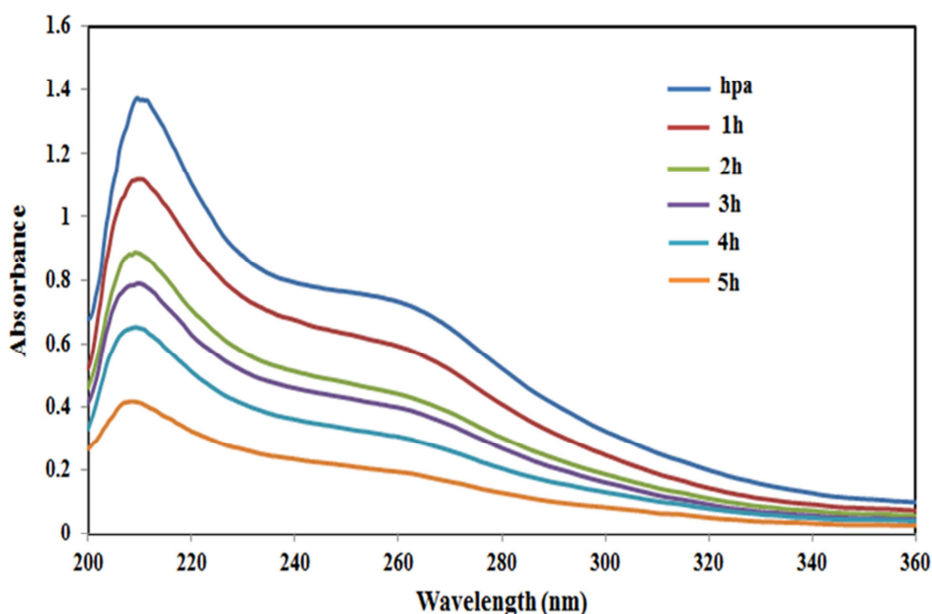


Figure 4. Evolution of UV-Vis spectra during $\text{H}_5\text{PW}_{10}\text{V}_2\text{O}_{40}$ addition to $\text{VO}_x/\text{SBA-15-NH}_2$.

The surface morphology of the $\text{H}_5\text{PW}_{10}\text{V}_2\text{O}_{40}@/\text{VO}_x/\text{SBA-15-NH}_2$ material was further investigated by FE-SEM (**Figure 5a,b**), which visualized irregular, micron-scale aggregates comprised of approximately 25 nm spherical nanoparticles possessing a narrow size distribution. Functionalization by 3-(triethoxysilyl)propylamine and subsequent HPA immobilization had minimal impact on the parent $\text{VO}_x/\text{SBA-15}$ morphology. Moreover, to establish the chemical

composition of the nanohybrid catalyst, $\text{HPA}@V\text{O}_x/\text{SBA-15-NH}_2$, energy dispersive X-ray (EDX) analysis was also compiled (**Figure 5c**). The EDX analysis showed the presence of tungsten in addition to vanadium and silicon in the nanocatalyst framework, indicating that vanadium and silicotungstic acid were successfully grafted onto SBA-15 mesoporous silica in accordance with ICP.

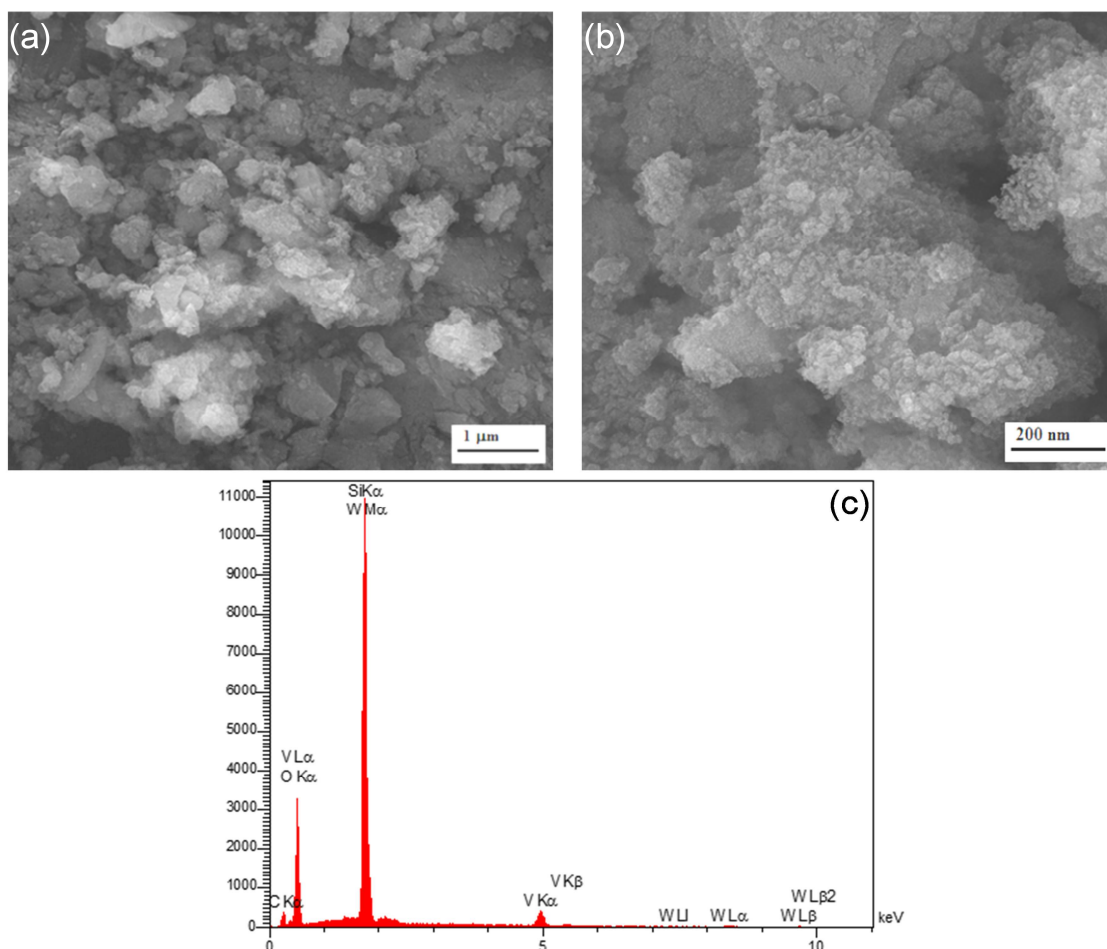


Figure 5. (a-b) FESEM micrograph and (c) corresponding EDX spectrum of $\text{H}_5\text{PW}_{10}\text{V}_2\text{O}_{40}@V\text{O}_x/\text{SBA-15-NH}_2$.

Surface properties of the mesoporous silicas were probed by FT-IR between 400-1400 cm^{-1} (**Figure 6**), to confirm the successful incorporation of NH_2 and HPA functionalities. The parent $\text{VO}_x/\text{SBA-15}$ exhibited a strong band around 1080 and a weak feature at 806 cm^{-1}

attributed to the asymmetric and symmetric Si–O–Si stretching vibrations respectively,⁵⁰ while a weak shoulder $\sim 960\text{ cm}^{-1}$ has been previously associated with vibrations of $[\text{SiO}_4]$ units bound to vanadium (Si–O–V) in vanadium modified MCM-41⁵¹. A broad band centered around 3500 cm^{-1} due to surface Si–OH and V–OH groups was also observed.⁵² Evidence for successful amine functionalization was indicated by the appearance of additional C–H and N–H stretches around 2929 and 1652 cm^{-1} respectively in the $\text{VO}_x/\text{SBA-15-NH}_2$ sample. Subsequent HPA functionalization conferred additional fingerprint bands at 1084 , 940 , 890 , and 796 cm^{-1} characteristic of the primary Keggin unit (**Figure S3**):^{53,54} the 1084 cm^{-1} band is attributed to symmetric stretching of PO_4 tetrahedra; that at 940 cm^{-1} to W–O_d stretches of the terminal oxygens; the 890 cm^{-1} band to W–O_b–W stretches associated with corner bridged oxygens; and the band at 796 cm^{-1} to W–O_c–W vibrations associated with side bridged oxygens.⁵⁵⁻⁵⁷ Note that identification of HPA vibrations is hindered by overlap of the W–O–W and P–O bands with contributions from Si–O–Si stretches in the underlying $\text{VO}_x/\text{SBA-15}$ support.

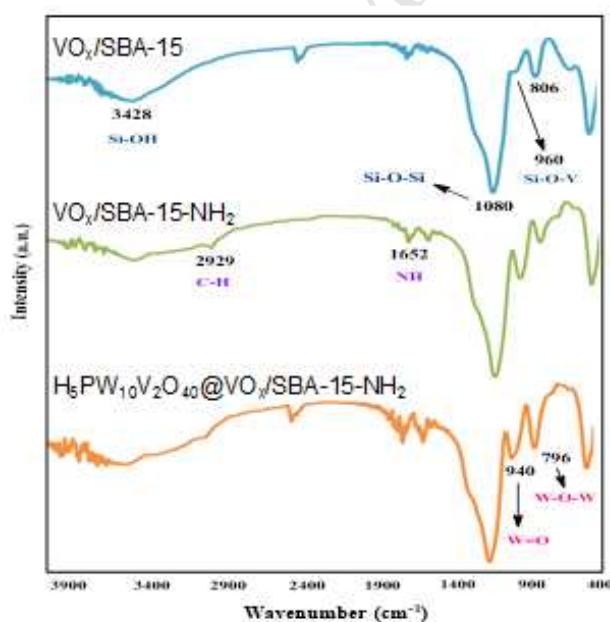


Figure 6. FT-IR spectra of functionalized SBA-15.

2.2 Catalytic synthesis of 3-substituted indoles

2-((1H-indol-3-yl)(phenyl)methyl)malononitrile synthesis from benzaldehyde, indole, and malononitrile was first investigated over $\text{H}_5\text{PW}_{10}\text{V}_2\text{O}_{40}@VO_x/\text{SBA-15-NH}_2$ in the absence of solvent at 50 °C. Only 10 % of the 3-substituted indole product was formed in the absence of a catalyst, even after the extended reaction time of 90 min (**Table 2**). In contrast, almost stoichiometric yields of 2-((1H-indol-3-yl)(phenyl)methyl)malononitrile were observed in the presence of 30 mg $\text{H}_5\text{PW}_{10}\text{V}_2\text{O}_{40}@VO_x/\text{SBA-15-NH}_2$ after only 20 min reaction (**Figure S4**), although additional catalyst had minimal impact with a plateau attained at 95 % yield for ≥ 30 mg. The effect of reaction temperature on the condensation of benzaldehyde, indole, and malononitrile was also studied (**Figure S5**), revealing a maximum around 50 °C, with a decrease at higher temperature associated with formation of the undesired by-product bis(indolyl)methane.^{39,40} The catalytic activity of the components constructing $\text{H}_5\text{PW}_{10}\text{V}_2\text{O}_{40}@VO_x/\text{SBA-15-NH}_2$, including $\text{H}_5\text{PW}_{10}\text{V}_2\text{O}_{40}$, $VO_x/\text{SBA-15-NH}_2$ and $VO_x/\text{SBA-15}$, were independently tested in the preparation of 2-((1H-indol-3-yl)(phenyl)methyl)malononitrile under the standard reaction conditions (**Table 2**). Immobilizing the heteropolyacid onto the modified material, $VO_x/\text{SBA-15-NH}_2$ increased the dispersion of the catalytically active Brønsted acid sites throughout the silica pore network, and hence increased activity. Hot filtration tests evidenced negligible leaching of any catalytically active components. In these tests, a reaction was carried out at 50 °C for 10 min in the presence of the $\text{H}_5\text{PW}_{10}\text{V}_2\text{O}_{40}@VO_x/\text{SBA-15-NH}_2$ catalyst, at which point the product yield reached 45 %. Ethanol was then added to the reaction mixture, and the catalyst removed immediately by filtration; the remaining filtrate was monitored for an additional 30 min at reaction temperature, however no further increase in product yield was observed, confirming the heterogeneous nature of the catalysis. The reproducibility and recyclability of $\text{H}_5\text{PW}_{10}\text{V}_2\text{O}_{40}@VO_x/\text{SBA-15-NH}_2$ for 2-((1H-indol-3-yl)(phenyl)methyl)malononitrile production was also assessed. A triplicate reaction evidenced product yields were reproducible within ± 2 % error. Catalyst re-use was assessed by filtering the $\text{H}_5\text{PW}_{10}\text{V}_2\text{O}_{40}@VO_x/\text{SBA-15-NH}_2$ catalyst after one reaction, washing it repeatedly with ethanol to remove residual organic species and subsequent drying at 90 °C for 4 h, and then adding to a fresh solution of the reaction mixture. Excellent catalyst stability was also observed from recycle experiments in which a smaller mass of catalyst was employed, and then spent catalyst recovered by filtration, washed with ethanol and dried at 110 °C for 2 h, and subsequently added to a fresh reaction mixture of the benzaldehyde, indole, and malononitrile.

Production of 2-((1H-indol-3-yl)(phenyl)methyl)malononitrile decreased by only 10 % over 8 consecutive re-uses (**Figure S6**). The FT-IR spectrum of the spent $\text{H}_5\text{PW}_{10}\text{V}_2\text{O}_{40}@VO_x/\text{SBA-15-NH}_2$ catalyst after 8 re-uses was identical to that of the as-prepared material, confirming preservation of the parent Keggin structure (**Figure S7**) and its immobilization over the amine-functionalized $\text{VO}_x/\text{SBA-15}$ support.

Table 2. Effect of catalyst mass on 2-((1H-indol-3-yl)(phenyl)methyl)malononitrile synthesis

Sample	Mass / mg	Reaction time / min	Product yield / %
0		90	10
$\text{H}_5\text{PW}_{10}\text{V}_2\text{O}_{40}$	8.1	20	48
$\text{VO}_x/\text{SBA-15}$	17.8	20	55
$\text{VO}_x/\text{SBA-15-NH}_2$	22	20	67
$\text{H}_5\text{PW}_{10}\text{V}_2\text{O}_{40}@VO_x/\text{SBA-15-NH}_2$	10	20	87
$\text{H}_5\text{PW}_{10}\text{V}_2\text{O}_{40}@VO_x/\text{SBA-15-NH}_2$	20	20	90
$\text{H}_5\text{PW}_{10}\text{V}_2\text{O}_{40}@VO_x/\text{SBA-15-NH}_2$	30	20	95
$\text{H}_5\text{PW}_{10}\text{V}_2\text{O}_{40}@VO_x/\text{SBA-15-NH}_2$	40	20	95
$\text{H}_5\text{PW}_{10}\text{V}_2\text{O}_{40}@VO_x/\text{SBA-15-NH}_2$	50	20	95

Reaction conditions: Benzaldehyde (1.0 mmol), indole (1.0 mmol), malononitrile (1.0 mmol) and the nanocatalyst were mixed to form a uniform liquid mixture which was stirred at 50 °C for the appropriate time. The progress of the reaction was monitored by TLC. Work-up was carried out as described in the experimental section.

The catalytic performance of $\text{H}_5\text{PW}_{10}\text{V}_2\text{O}_{40}@VO_x/\text{SBA-15-NH}_2$ was benchmarked against literature metal oxides previously reported for similar condensations (**Table 3**), from which it is evident that only TiO_2 modified clinoptilolite offers a comparable yield to that of our supported HPA system.

Table 3. Catalyst performance in 2-((1H-indol-3-yl)(phenyl)methyl)malononitrile synthesis.

Catalyst	Yield / %
$\text{H}_5\text{PW}_{10}\text{V}_2\text{O}_{40}@10\%VO_x/\text{SBA-15-NH}_2$	95
SBA-15	55
V/SBA-15	80
MCM-41	50
TiO_2 -clinoptilolite	87
Clinoptilolite	65
ReO	70
ZnO	74

TiO ₂	70
CeO ₂	68

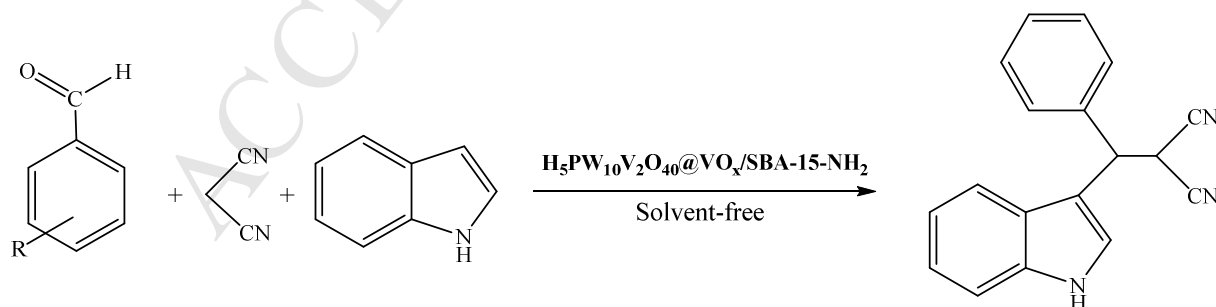
0.3 mmol of each catalyst was utilized in all cases. 0.03 g of the nanohybrid catalyst was used. All of them was conducted at 20 min. ReO refers to a rare earth oxide mixture including La₂O₃ and Ce₂O₃. Yield% refers to the isolated yield.

An E-factor analysis employing the method proposed by Sheldon^{58,59} highlights the excellent atom efficiency of the condensation reaction. For 1 mmol benzaldehyde, 1 mmol indole and 1 mmol malononitrile reacting over H₅PW₁₀V₂O₄₀@VO_x/SBA-15-NH₂ under solvent-free conditions the E-factor is calculated below at 0.13. This compares very favorably with alternative literature systems for the same reaction (**Table S1**), which vary between 0.13 and 150 and require extended reaction times spanning 2 to 48 h (versus 20 min in this work):

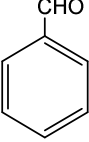
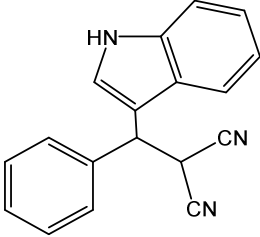
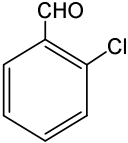
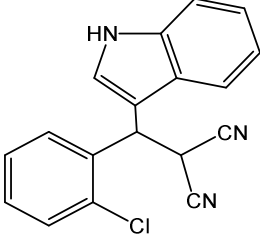
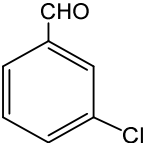
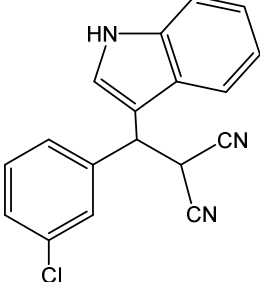
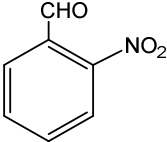
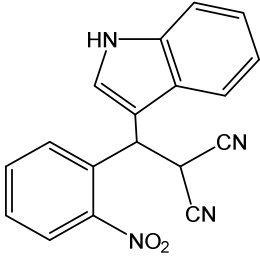
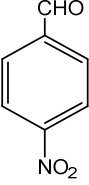
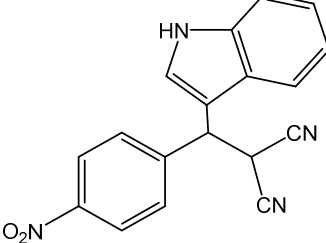
$$\text{E-factor} = [(0.106 \text{ g benzaldehyde} + 0.117 \text{ g indole} + 0.066 \text{ g malononitrile}) - 0.256 \text{ g product}] / 0.256 \text{ g product} = 0.13$$

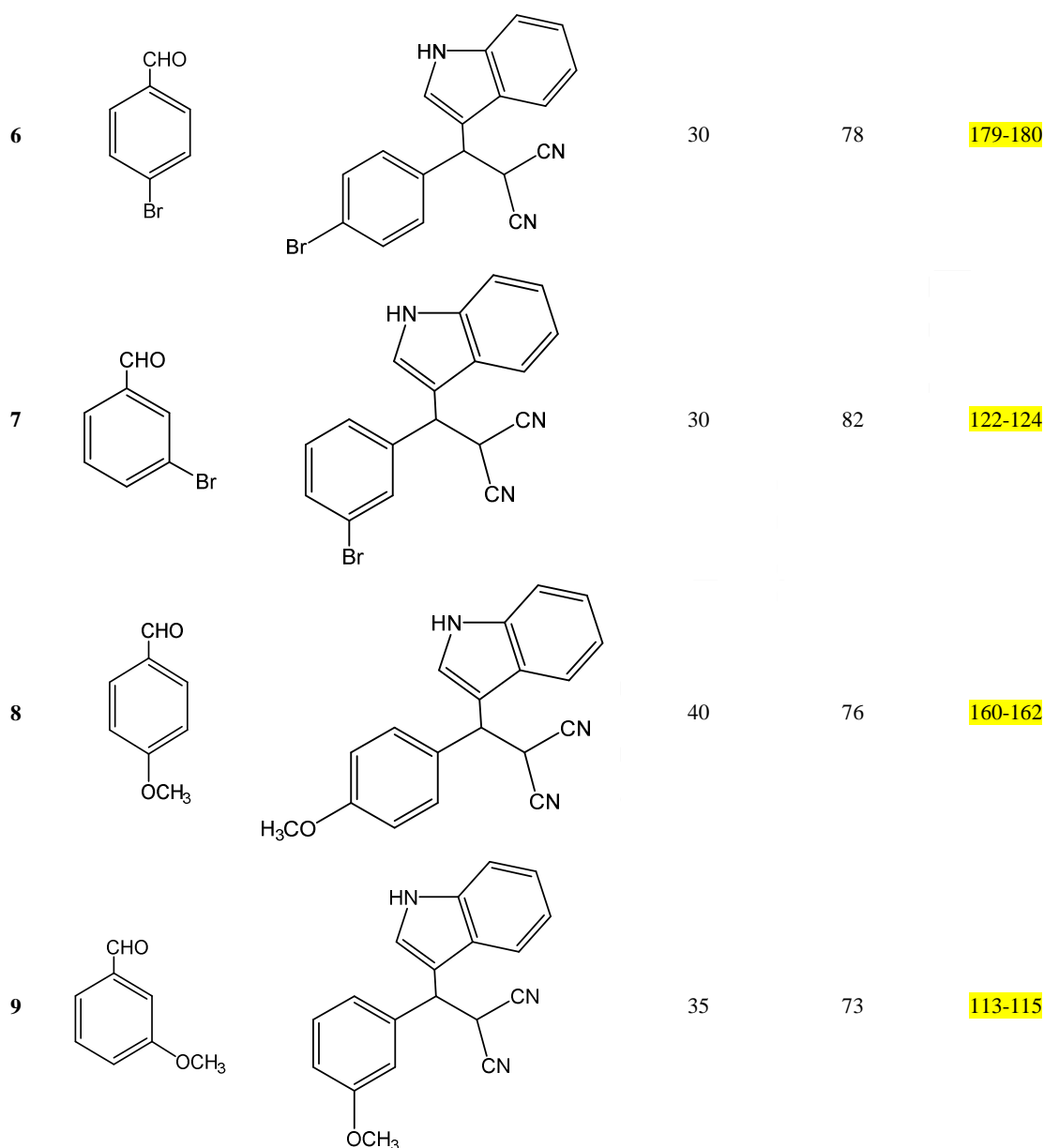
The efficacy of H₅PW₁₀V₂O₄₀@VO_x/SBA-15-NH₂ for the generic synthesis of 3-substituted indoles from diverse aromatic aldehydes possessing electron withdrawing or donating substituents was also studied.^{38,39} **Table 4** demonstrates that high yields were obtained for most of the aromatic aldehydes, with electron-withdrawing groups affording slightly enhanced yields of 78-95 % (**entries 1-7**) relative to electron-donating groups (73-76 %, **entries 8-9**).

Table 4. Synthesis of 3-substituted indoles over H₅PW₁₀V₂O₄₀@10%VO_x/SBA-15-NH₂



R= electron-withdrawing (donating) group

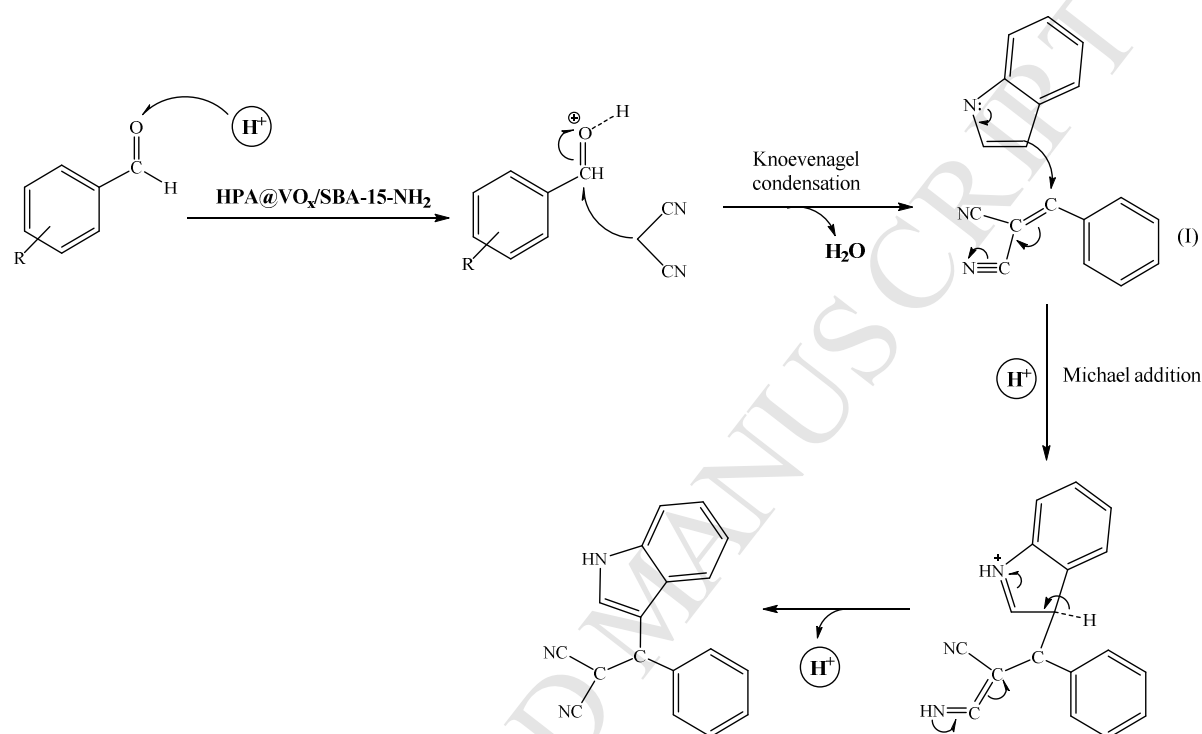
Entry	Aldehyde	Product	Reaction time	Product yield	Melting point
			/ min	/ %	/ °C
1			20	95	79-80
2			35	85	113-115
3			15	95	173-175
4			30	89	135-137
5			20	91	160-162



Reaction conditions are provided in **Table 1**.

A plausible reaction mechanism for the reaction of benzaldehyde, indole, and malononitrile is shown in **Scheme 3**, beginning with a Knoevenagel condensation to form (I) via nucleophilic addition of malononitrile to the carbonyl group of the aldehyde. The indole may subsequently react with (I) through a Michael addition to afford the desired 2-((1H-indol-3-yl)(phenyl)methyl)malononitrile product. We propose that the heteropolyacid protonates the

carbonyl of the aromatic aldehyde thereby increasing its Lewis acidity: electron-donating substituents deactivate the aldehyde to nucleophilic attack by the malononitrile, while in contrast electron- withdrawing groups activate the aldehyde carbonyl.^{60,39}



Scheme 3. Plausible mechanism for the synthesis of 3-substituted indoles.

3. Conclusions

A bifunctional, mesoporous solid acid catalyst was synthesized incorporating both vanadate and heteropolyacid functions, the latter immobilized via a 3-(triethoxysilyl)propylamine linker. The structure of the resulting catalyst was fully characterized by bulk and surface analytical techniques, which confirmed preservation of the $\text{H}_5\text{PW}_{10}\text{V}_2\text{O}_{40}$ following its immobilization. The resulting $\text{H}_5\text{PW}_{10}\text{V}_2\text{O}_{40}@VO_x/\text{SBA-15-NH}_2$ catalyst offers an atom efficient route to the one-pot preparation of 3-substituted indoles through the condensation of indole, malononitrile, and aromatic aldehydes under solvent-free and mild reaction conditions. A 95 % yield of 2-((1H-indol-3-yl)(phenyl)methyl)malononitrile was obtained from benzaldehyde in only 20 min at 50

°C, with the catalyst recyclable with negligible deactivation over 8 re-uses. $\text{H}_5\text{PW}_{10}\text{V}_2\text{O}_{40}@VO_x/\text{SBA-15-NH}_2$ is a versatile catalyst delivering yields of 3-substituted indoles between 70-95 % for a range of aromatic aldehydes possessing electron-withdrawing or -donating substituents, the former proving more reactive possibly due to activation of the carbonyl towards Knoevenagel condensation with malononitrile. The low E-factor and high activity of $\text{H}_5\text{PW}_{10}\text{V}_2\text{O}_{40}@VO_x/\text{SBA-15-NH}_2$ unlocks a new and attractive approach to the synthesis of biologically active 2-((1H-indol-3-yl)(phenyl)methyl)malononitrile and its analogues.

4. Experimental

4.1 General information

Starting materials and solvents for catalyst synthesis were from commercial sources and utilized as obtained, with the exception of $\text{VO}(\text{O-}^t\text{Bu})_3$ which was prepared according to the literature.⁶¹

4.2 Characterization

Morphologies of the prepared materials were observed with a Mira 3-XMU Field emission scanning electron microscope (FE-SEM). Crystallinity was evaluated by powder X-ray diffraction (XRD) on a PW1800-PHILIPS diffractometer with Cu K_α radiation ($\lambda = 1.5418 \text{ \AA}$) at 40 kV and 30 mA. Fourier transform infrared (FT-IR) spectra were recorded on an 8700 Shimadzu Fourier Transform spectrophotometer between 400 to 4000 cm^{-1} employing samples diluted in KBr pellets. Thermogravimetric and differential thermal analysis (TGA-DTA) was performed on a Bahr STA-503 instrument in air at a heating rate of 10 $^\circ\text{C}/\text{min}^{-1}$. Ultraviolet-visible (UV-Vis) spectra were obtained on a Shimadzu Model UV-2550 spectrophotometer. Melting points were recorded on a Bamstead electrothermal type 9200 melting point apparatus. ^1H - and ^{13}C -NMR spectra were recorded on a Bruker AVANCE 300 MHz spectrometer using TMS as an internal reference. Elemental analysis was performed with a Thermo Finnigan Flash-1112EA microanalyzer and a Varian Vista-PRO ICP-OES. Porosimetry measurements were conducted by N_2 physisorption on a Quantachrome Nova 4200e porosimeter with data analysis employing Novawin v11.0 software: samples were degassed at 120 $^\circ\text{C}$ for 4 h prior to analysis by nitrogen adsorption at -196 $^\circ\text{C}$, with BET surface areas calculated over the range $P/P_0 = 0.05$ -0.35 where a linear relationship was maintained, while pore size distributions were calculated

using the BJH model from the desorption isotherm. XPS analysis was performed on a Kratos Axis HSi photoelectron spectrometer equipped with a charge neutralizer and magnetic focusing lenses, employing monochromatic Al K_{α} radiation (1486.6 eV) with energy referencing to the C 1s peak at 284.8 eV.

4.3 Preparation of $VO_x/SBA-15$

Vanadium modified SBA-15 was prepared using tetraethylorthosilicate (TEOS, Sigma Aldrich 99 %) as a silica source and Pluronic P123 ($M_{av}= 5,800$, Sigma Aldrich) as a structure directing agent, and vanadium(V) oxytri-tert-butoxide as the vanadium precursor. Incorporation of vanadium alkoxide in the siliceous framework was achieved in-situ. In a typical synthesis, P123 (3.0 g) was dissolved in deionized water (69 mL) to obtain a transparent solution; separately TEOS (6.9 g) was added to deionized water (20 mL), and the resultant mixture added dropwise to the surfactant solution and aged at 40 °C for 10 min. The desired quantity of vanadium alkoxide (3 and 6 mmol) was then introduced to the aged mixture to obtain a nominal V:Si molar ratio of 10. An appropriate amount of 0.30 M aqueous HCl was then added to adjust the pH to 3. Finally, the resulting blend was stirred for 2 h at 40 °C and then transferred to a Teflon lined autoclave and heated to 100 °C for 48 h. The resultant precipitate was filtered, washed with deionized water until a neutral filtrate was obtained, and dried at room temperature overnight. The organic surfactant was removed by calcination in static air at 540 °C (ramp rate 3 °C/min) for 6 h to yield the mesoporous $VO_x/SBA-15$ (I).

4.4 Surface modification of $VO_x/SBA-15$ by 3-(triethoxysilyl)propylamine and $H_5PW_{10}V_2O_{40}$

Amine functionalized $VO_x/SBA-15$ (II) was prepared by dispersing the parent $VO_x/SBA-15$ (1.0 g) in toluene (30-40 mL) by 30 min ultrasonication. Subsequently, 3-(triethoxysilyl)propylamine (1.40 mL) was added to the suspension and refluxed for 24 h. The resulting $VO_x/SBA-15-NH_2$ was separated by filtration, washed with acetone, and dried at room temperature. $H_5PW_{10}V_2O_{40}$ was prepared according to the earlier reports⁶² and immobilized on $VO_x/SBA-15-NH_2$ by the addition of HPA (0.4 g) to the mesoporous silica (0.8 g) in methanol (50 mL) and subjected to 5 h reflux. The final material was filtered and washed with methanol repeatedly (until the filtrate became clear) and finally dried at room temperature. The overall catalyst synthesis is depicted in **Scheme 2**.

4.5 Catalytic synthesis of 2-((1H-indol-3-yl)(aryl)methyl)malononitriles

H₅PW₁₀V₂O₄₀@VO_x/SBA-15-NH₂ (30 mg) was added to a mixture of aldehyde (1.0 mmol), indole (1.0 mmol) and malononitrile (1.0 mmol) and heated to 50 °C. Aldehyde (liquid and/or solid), indole (solid, m.p. 52–53 °C) and malononitrile (freshly crystallized) and the catalyst formed a dense liquid with a total volume of ~0.3 mL. The progress of reactions was monitored by TLC (n-hexane:ethylacetate, 3:2 molar ratio), and on their completion, hot ethanol (3 mL) was added to the reaction mixture and stirred for 10 min. The heterogeneous catalyst was then quickly filtered and the filtrate cooled to 5 °C to precipitate the product which was then purified by filtration of any unreacted (soluble) reactants. Products were characterized by comparison of their physical data with those of known 2-((1H-indol-3-yl)(aryl)methyl)malononitriles.^{59,63,37-40,64}

Acknowledgements

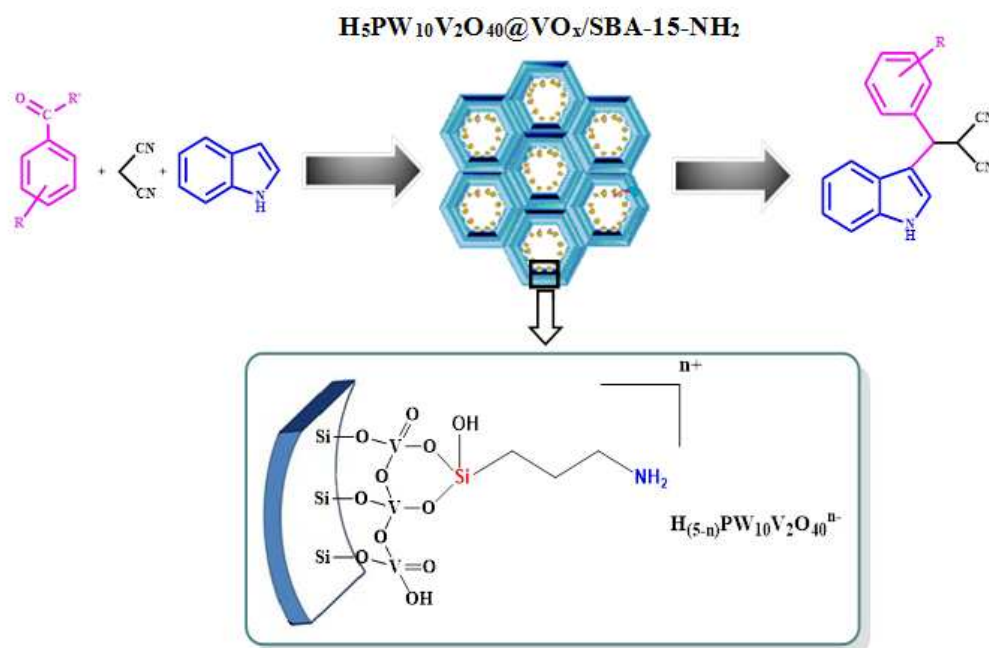
We thank the Research Councils of Hakim Sabzevari and Shahid Beheshti Universities for partial financial support.

References

1. Dai, L.-X.; Tabata, K.; Suzuki, E.; Tatsumi, T. *Chem. Mater.* 2001;13:208-212.
2. Vinu, A.; Hossain, K. Z.; Ariga, K. *J. Nanosci. Nanotechnol.* 2005;5:347-371.
3. Taguchi, A.; Schüth, F. *Micropor. Mesopor. Mat.* 2005;77:1-45.
4. Lee, A. F.; Bennett, J. A.; Manayil, J. C.; Wilson, K. *Chem. Soc. Rev.* 2014;43:7887-7916.
5. Parlett, C. M. A.; Wilson, K.; Lee, A. F. *Chem. Soc. Rev.* 2013;42:3876-3893.
6. Gao, X.; Bare, S. R.; Weckhuysen, B. M.; Wachs, I. E. *J. Phys. Chem B.* 1998;102:10842-10852.
7. Hess, C.; Hoefelmeyer, J. D.; Tilley, T. D. *J. Phys. Chem. B.* 2004;108:9703-9709.
8. Meynen, V.; Cool, P.; Vansant, E.; Kortunov, P.; Grinberg, F.; Kärger, J.; Mertens, M.; Lebedev, O.; Van Tendeloo, G. *Micropor Mesopor Mat.* 2007;99:14-22.
9. Gao, F.; Zhang, Y.; Wan, H.; Kong, Y.; Wu, X.; Dong, L.; Li, B.; Chen, Y. *Micropor Mesopor Mat.* 2008;110:508-516.
10. Meynen, V.; Cool, P.; Vansant, E. *Micropor Mesopor Mat.* 2009;125:170-223.
11. Osatiashtiani, A.; Lee, A. F.; Granollers, M.; Brown, D. R.; Olivi, L.; Morales, G.; Melero, J. A.; Wilson, K. *ACS Catal.* 2015;5:4345-4352.
12. Creasey, J. J.; Parlett, C. M. A.; Manayil, J. C.; Isaacs, M. A.; Wilson, K.; Lee, A. F. *Green Chem.* 2015;17:2398-2405.
13. Ryoo, R.; Kim, M. J. *Chem. Commun.* 1997;2225-2226.
14. Liu, Y.-M.; Cao, Y.; Yi, N.; Feng, W.-L.; Dai, W.-L.; Yan, S.-R.; He, H.-Y.; Fan, K.-N. *J. Catal.* 2004;224:417-428.

15. Hess, C.; Looi, M. H.; Hamid, S. B. A.; Schlögl, R. *Chem. Commun.* 2006;451-453.
16. Udayakumar, V.; Pandurangan, A. *J Porous Mat.* 2014;21:921-931.
17. Wachs, I. E. *Dalton T.* 2013;42:11762-11769.
18. Jermy, B. R.; Kim, S.; Kim, D.; Park, D. *J. Ind. Eng. Chem.* 2011;17:130-137.
19. Du, G.; Lim, S.; Pinault, M.; Wang, C.; Fang, F.; Pfefferle, L.; Haller, G. L. *J. Catal.* 2008;253:74-90.
20. Wang, G.; Zhang, S.; Huang, Y.; Kang, F.; Yang, Z.; Guo, Y. *Appl. Catal. A Gen.* 2012;413:52-61.
21. Cavani, F.; Ballarini, N.; Cericola, A. *Catal Today.* 2007;127:113-131.
22. Piumetti, M.; Bonelli, B.; Massiani, P.; Millot, Y.; Dzwigaj, S.; Gaberova, L.; Armandi, M.; Garrone, E. *Micropor Mesopor Mat.* 2011;142:45-54.
23. Piumetti, M.; Bonelli, B.; Armandi, M.; Gaberova, L.; Casale, S.; Massiani, P.; Garrone, E. *Micropor Mesopor Mat.* 2010;133:36-44.
24. Rossetti, I.; Fabbrini, L.; Ballarini, N.; Oliva, C.; Cavani, F.; Cericola, A.; Bonelli, B.; Piumetti, M.; Garrone, E.; Dyrbeck, H. *J. Catal.* 2008;256:45-61.
25. Piumetti, M.; Bonelli, B.; Massiani, P.; Dzwigaj, S.; Rossetti, I.; Casale, S.; Gaberova, L.; Armandi, M.; Garrone, E. *Catal Today.* 2011;176:458-464.
26. Chiesa, M.; Meynen, V.; Van Doorslaer, S.; Cool, P.; Vansant, E. F. *J. Am. Chem. Soc.* 2006;128:8955-8963.
27. Jermy, B. R.; Kim, S.-Y.; Bineesh, K. V.; Park, D.-W. *Micropor Mesopor Mat.* 2009;117:661-669.
28. Luan, Z.; Bae, J. Y.; Kevan, L. *Chem. Mater.* 2000;12:3202-3207.
29. Luan, Z.; Hartmann, M.; Zhao, D.; Zhou, W.; Kevan, L. *Chem. Mater.* 1999;11:1621-1627.
30. Hamilton, N.; Wolfram, T.; Müller, G. T.; Hävecker, M.; Kröhnert, J.; Carrero, C.; Schomäcker, R.; Trunschke, A.; Schlögl, R. *Catal. Sci. Tech.* 2012;2:1346-1359.
31. Tsoncheva, T.; Ivanova, L.; Dimitrova, R.; Rosenholm, J. *J. Colloid Interface Sci.* 2008;321:342-349.
32. Mizuno, N.; Misono, M. *Chem. Rev.* 1998;98:199-218.
33. Frattini, L.; Isaacs, M. A.; Parlett, C. M. A.; Wilson, K.; Kyriakou, G.; Lee, A. F. *Appl. Catal., B.* 2017;200:10-18.
34. Tayebbe, R.; Amini, M. M.; Ghadamgahi, M.; Armaghan, M. *J. Mol. Catal. A Chem.* 2013;366:266-274.
35. Rajesh, U. C.; Wang, J.; Prescott, S.; Tsuzuki, T.; Rawat, D. S. *ACS. Sustain. Chem. Eng.* 2014;3:9-18.
36. Kumar, A.; Gupta, M. K.; Kumar, M. *Green Chem.* 2012;14:290-295.
37. Qu, Y.; Ke, F.; Zhou, L.; Li, Z.; Xiang, H.; Wu, D.; Zhou, X. *Chem. Commun.* 2011;47:3912-3914.
38. Wang, L.; Huang, M.; Zhu, X.; Wan, Y. *Appl. Catal. A Gen.* 2013;454:160-163.
39. He, Y.-H.; Cao, J.-F.; Li, R.; Xiang, Y.; Yang, D.-C.; Guan, Z. *Tetrahedron.* 2015;71:9299-9306.
40. Anselmo, D.; Escudero - Adán, E. C.; Martínez Belmonte, M.; Kleij, A. W. *Eur. J. Inorg. Chem.* 2012;2012:4694-4700.
41. Segura, Y.; Cool, P.; Kustrowski, P.; Chmielarz, L.; Dziembaj, R.; Vansant, E. *J. Phys. Chem. B.* 2005;109:12071-12079.
42. Hess, C.; Schlögl, R. *Chem. Phys. Lett.* 2006;432:139-145.
43. Piumetti, M.; Bonelli, B.; Massiani, P.; Dzwigaj, S.; Rossetti, I.; Casale, S.; Armandi, M.; Thomas, C.; Garrone, E. *Catal Today.* 2012;179:140-148.
44. ALOthman, Z. A. *Materials.* 2002;5:2874-2902.
45. Wainwright, S. G.; Parlett, C. M. A.; Blackley, R. A.; Zhou, W.; Lee, A. F.; Wilson, K.; Bruce, D. W. *Micropor Mesopor Mat.* 2013;172:112-117.
46. Tarlani, A.; Abedini, M.; Nemat, A.; Khabaz, M.; Amini, M. M. *J. Colloid. Interface. Sci.* 2006;303:32-38.

47. Chen, X.; Zhao, W.; Wang, F.; Xu, J. *J. Nat. Gas. Chem.* 2012;21:481-487.
48. NIST X-ray Photoelectron Spectroscopy Database, Version 4.1 (National Institute of Standards and Technology, Gaithersburg, 2012); <http://srdata.nist.gov/xps/>.
49. Tayebee, R.; Amini, M. M.; Rostamian, H.; Aliakbari, A. *Dalton Trans.* 2014;43:1550-1563.
50. Kong, Y.; Zhu, H.; Yang, G.; Guo, X.; Hou, W.; Yan, Q.; Gu, M.; Hu, C. *Adv. Funct. Mater.* 2004;14:816-820.
51. Luan, Z.; Xu, J.; He, H.; Klinowski, J.; Kevan, L. *J. Phys. Chem. A.* 1996;100:19595-19602.
52. Van Der Voort, P.; White, M.; Mitchell, M.; Verberckmoes, A.; Vansant, E. *Spectrochim. Acta Mol. Biomol. Spectrosc.* 1997;53:2181-2187.
53. Pope, M. T. *Heteropoly and isopoly oxometalates*; Springer Verlag. 1983;8.
54. Newman, A. D.; Lee, A. F.; Wilson, K.; Young, N. A. *Catal Letters.* 2005;102:45-50.
55. Kim, H.-J.; Shul, Y.-G.; Han, H. *Appl. Catal. A Gen.* 2006;299:46-51.
56. Tayebee, R.; Amini, M. M.; Nehzat, F.; Sadeghi, O.; Armaghan, M. *J. Mol. Catal. A Chem.* 2013; 366:140-148.
57. Pamin, K.; Kubacka, A.; Olejniczak, Z.; Haber, J.; Sulikowski, B. *Appl. Catal. A Gen.* 2000;194-195:137-146.
58. Sheldon, R. *Chem. Commun.* 2001;2399-2407.
59. Hasaninejed, A.; Kazerooni, M. R.; Zare, A. *Catal Today.* 2012;196:148-155.
60. Rajesh, U. C.; Kholiya, R.; Thakur, A.; Rawat, D. S. *Tetrahedron Lett.* 2015;56:1790-1793.
61. Pak, C.; Bell, A. T.; Tilley, T. D. *J. Catal.* 2002;206:49-59.
62. Tayebee, R.; Tizabi, S. *Chinese. J. Catal.* 2012;33:923-932.
63. Amrollahi, M. A.; Kheilkordi, Z. *J. Iran. Chem. Soc.* 2016;13:925-929.
64. Chandrasekhar, S.; Patro, V.; Reddy, G. P. K.; Grée, R. *Tetrahedron Lett.* 2012;53:6223-6225.



Graphical Abstract

$H_5PW_{10}V_2O_{40}@VO_x/SBA-15-NH_2$ was prepared, characterized, and introduced as an effective catalyst for the one-pot synthesis of 3-substituted indoles. The catalyst could be easily separated without noticeable reduction in activity.

- An inorganic-organic nanoporous material $\text{H}_5\text{PW}_{10}\text{V}_2\text{O}_{40}@VO_x/\text{SBA-15-NH}_2$ is synthesised
- An efficient and environmentally benign route to 3-substituted indoles is shown
- $\text{H}_5\text{PW}_{10}\text{V}_2\text{O}_{40}@VO_x/\text{SBA-15-NH}_2$ offers wide scope for a variety of aldehyde substrates